JOURNAL OF MATERIALS SCIENCE 30 (1995) 4994–5001

Effect of weak uniaxial loads on creep strain rate in high-porosity MgO compacts during early sintering stages

D. BERUTO*, M. CAPURRO*, R. NOVAKOVIC, R. BOTTER*
*Inter-department Center of Materials Engineering (CIIM), and *Instituto di Ingegneria e Scienza dei Materiali, Faculty of Engineering, University of Genoa, Genoa, Italy*

Creep phenomena accompanying the early stage of sintering of high-porosity MgO powder compacts were investigated with regard to the dependence of creep rate on the applied stress. This dependence was found to be non-linear, obeying a power law with an exponent $n < 1$, in contrast with the behaviour of dense compacts which exhibit linear Nabarro–Herring creep under the same type of loading. The nature of the creep exponent, expected to be in relation to mechanisms of particle disconnection and rearrangement, frequently observed in a high-porosity compact during the early stage of neck formation, has been explored using an appropriate physico-mathematical model. The relevant point concerning high-porosity compacts is that, owing to the loosely packed microstructure, the necks must resist not only normal forces, but also bending moments. It is the action of such bending moments which is supposed to drive the particles rearrangement. In this framework, the nature of the creep exponent appears to be related mainly to the green density, but it is substantially constant with densification. The predictions of the model explain the experimental results for $n < 1$ (high-porosity green compacts), with a smooth transition to the case of $n = 1$ (low-porosity green compacts).

1. Introduction

Dilatometric experiments show that high-porosity compacts fired under weak uniaxial forces, undergo densification and creep. Rahaman and co-workers [1–7] have proved for a number of ceramics compacts that the densification rate is practically unaffected by the action of weak uniaxial loads. In this way the creep time history can be derived from separate measurements of total axial shrinkage on loaded and unloaded samples [8]. Creep tests under different loads can be carried out to investigate the dependence of the creep rate on the applied compressive stress, σ_0, and on temperature.

In a recent research on low-density MgO compacts [9], the dependence of the densification and creep rates (respectively $\dot{\varepsilon}_d$ and $\dot{\varepsilon}_c$) on temperature and microstructure, was investigated. For compacts of this kind the microstructure was shown to be entirely described in terms of the actual density. Thus, fixing density, the true temperature dependence of both densification and creep rate, could be enucleated and was shown to be the same. On the other hand, the two rates were found to be differently influenced by microstructure, in particular the creep rate appeared to decrease faster than the densification rate, as the relative density increased. This feature is peculiar to low-density compacts, because results obtained by other authors [1 – 7] on dense compacts indicate that the ratio of the two rates is approximately constant with density.

To explore the dependence of creep phenomena on microstructure in the case of low-density green bodies is not an easy task, because a number of matter transport phenomena, as well as mechanisms of particle rearrangement, are expected to be active in the early stages of isothermal sintering. Because these mechanisms are ordinarily cooperative, it is difficult to single out a dominant one in the creep behaviour. However, a contribution to such a complex field can be given by investigating the effect of the applied compressive stress on the creep rate.

The dependence of the creep rate on the applied stress is normally expressed by a law of the type

$$\dot{\varepsilon}_c = f(G, \rho, T)\,\sigma_0^n \qquad (1)$$

where $f(G, \rho, T)$ is a complicated function dependent on powder geometry (generically indicated by symbol G), microstructure (expressed by actual relative density, ρ, for the reason given above) and temperature, T, and the exponent n is related to the nature of the creep mechanism. Accordingly, if one compares creep results obtained under different applied stresses on samples with equal actual density, temperature and geometry, it is possible to determine the creep exponent in Equation 1. If the phenomenon is substantially amenable to a Nabarro–Herring creep, n should be

0022–2461

equal to 1, while $n > 1$ would indicate a behaviour in the plastic range [10].

Highly porous compacts, during the early stage of sintering, may undergo, due to inherent instabilities in the solid-pore phase, particle disconnections and rearrangement [11, 12]. These phenomena are related to the anisotropy of the neck growth as well as to the non-uniformity of the stress distribution acting on the neck cross-section of a loosely packed compact. As far as we are aware, the way how these phenomena can influence the value of the creep exponent, n, has never been reported, making the subject of the present investigation.

2. Experimental procedure

2.1. Materials

The magnesium ceramic oxide powders used to obtain porous compact samples, were prepared by decomposition of $Mg(OH)_2$ powders in air at 1173 K. Surface area values of the oxide powder were about 11 $m^2 g^{-1}$. Impurities were all below 2.5 p.p.m. SEM observations gave a mean grain size of 0.17 μm, from which a surface area of 10.9 $m^2 g^{-1}$ can be derived. Accordingly, the oxide powders produced by the decomposition reaction are not porous.

The porous compacts were produced in form of cylinders 8 mm diameter and 8 mm long from a slurry with ethyl alcohol, using a press-filtering method already described elsewhere [13].

The green density of pressed compacts was obtained both from direct measurements of mass and volume and also by the porosimetric technique. The experimental error of such measurements was within 0.5%; the mean relative green density for all samples was found to be 0.28 ± 0.005.

2.2. Specimen treatment

The samples were placed in a loading dilatometer, already described elsewhere [14]. The furnace was preheated at a heating rate of 20 K min^{-1}, in such a way as to obtain a central region 20 mm long where temperature was equal to 1298 ± 0.5 K. Dry nitrogen was flowing in the dilatometer at a rate of 200 mn min^{-1}. The external load was transmitted to the sample by an alumina pushing rod driven by a gas actuator and was applied from the beginning of the firing run. The calibration error of the loading device, including thermal effects on the actuator, was estimated in $\pm 10\%$ of the actual applied load. The nominal applied stress, σ_0, is calculated by dividing the force by the initial cross-sectional area of the sample.

Initially the samples were kept for 2 h in a region of the furnace where the temperature was about 673 K. This treatment was devised to eliminate the influence of the water vapour eventually contained in the sample on the sintering process [15]. The sample was then pushed into the hot zone at a pre-set temperature. A thermocouple, placed about 1 mm over the sample, permits evaluation of the duration of the non-isothermal period once the sample and the pushing rod are introduced in the hot isothermal region. This transitory period was found to be about 10 min. However, because the thermocouple is not directly attached to the sample, a delay must be expected [14] before the sample reaches the isothermal regime. The sintering temperature was selected in order both to obtain measurable changes of density in reasonably short firing times and to minimize the fraction of linear shrinkage occurring in the non-isothermal regime. The non-isothermal period was less than 20 min, for a total run of 120 min.

Fresh samples of equal size, composition and density were used for each applied load. The explored range of applied stress was 6.9–90 kPa. In order to have an applied effective stress as constant as possible during the densification process, the dimensional change of cross-sectional area of the samples was kept as low as possible. Tests were designed for a total amount of densification not higher than 20%–25%, so that the change in true stress due to change in cross-sectional area was within the experimental error ($\pm 10\%$) for the duration of the test.

The apparent density of the compact was determined for each applied stress before and after firing from direct measurement of sample geometry and mass.

The densification strain, ε_d, which should be independent of the applied stress, has been determined by measuring the relative density of equal fresh samples in a number of interrupted runs without external load. Agreement between the final value of relative density (0.353 at 120 min) measured in such a condition and that obtained in the presence of applied stresses, was reported to within a scatter of 6%–8%.

3. Results

Isotropic linear shrinkage ε_d ($\approx \Delta\rho/3\rho_0$ in the case of small deformations) and total axial shrinkage $\varepsilon = \Delta L/L_0$ are plotted against time in Fig. 1 for different applied loads. Density measurements were made with and without the dilatometer rod in place. The experimental error in green density amounts to $\pm 0.5\%$ of the 0.284 average value for all the samples used in

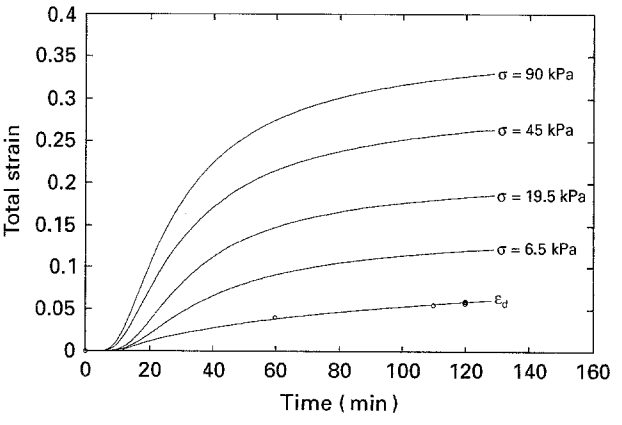

Figure 1 Total strain histories at different applied stresses and densification history. Experimental points (circled in the plot) derive from direct measurements of density.

the different runs, while the densities of the sintered samples were measured with an error of 4%–5% of the values in Fig. 1. Accordingly we can assume that also in the early stage of sintering, weak uniaxial loads have little or no influence on the densification process. This is also true of MgO compacts of the same green density sintered for longer times [9] and compares with the results of Rahaman and co-workers [1–7] on denser compacts.

The creep strain is calculated from total axial shrinkage and isotropic linear shrinkage as [16]

$$\varepsilon_c = \varepsilon - \varepsilon_d \tag{2}$$

Processing the data of Fig. 1 by means of Equation 2, creep curves plotting creep–strain against time are obtained and are given in Fig. 2. For all the applied loads, these curves exhibit an S-shape in the explored time range. Such curves obey a phenomenological equation of the type

$$\varepsilon_c = \frac{c}{a + \exp(-b/t)} \tag{3}$$

a, b and c being phenomenological constants calculated for each applied load.

The creep strain rate, $\dot{\varepsilon}_c$, is given by the time derivative of Equation 3 and the corresponding curves are shown in Fig. 3. The isothermal segment of the test, as remarked in the experimental section, is expected to start about 20 min from the beginning of the run. The

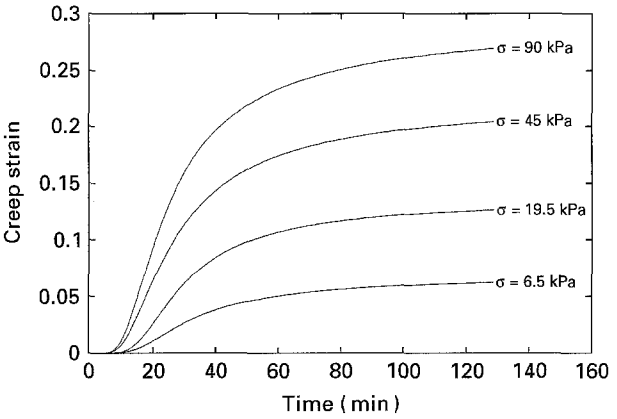

Figure 2 Creep-strain histories at different applied stresses.

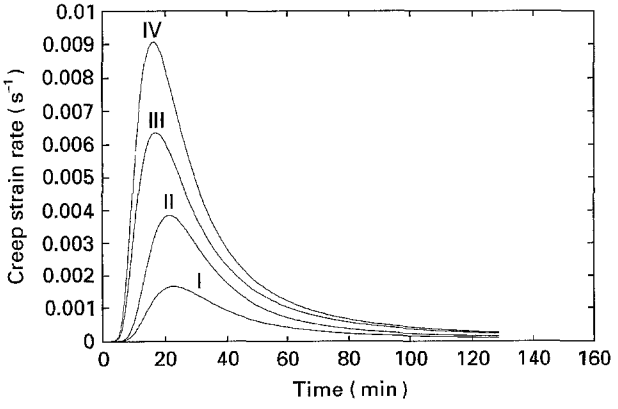

Figure 3 Creep strain rate versus time at different applied stresses: (I) 6.5 kPa, (II) 19.5 kPa, (III) 45 kPa, (IV) 90 kPa.

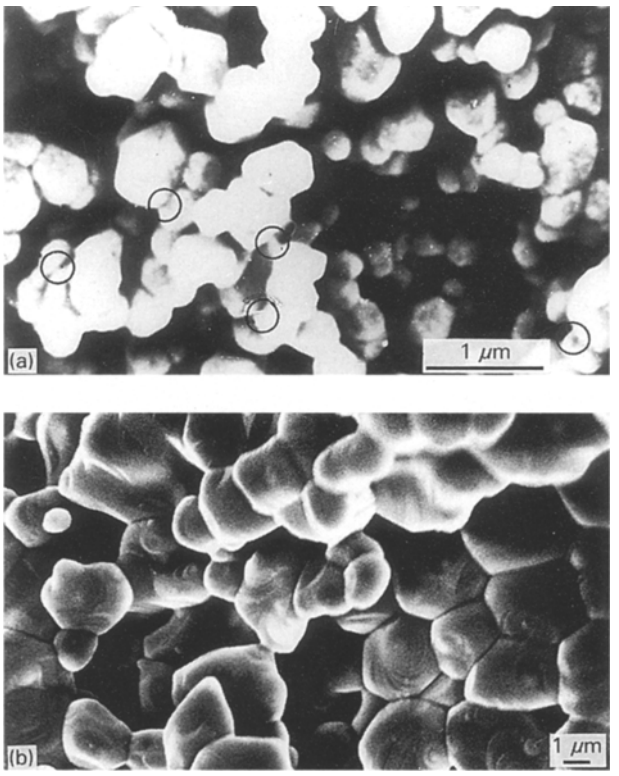

Figure 4 Microstructures of (a) high-porosity and (b) low-porosity compacts from SEM observations. Effects of grain-boundary disconnection and tilting circled in (a).

isothermal regime is characterized by an observed creep rate rapidly decaying to zero independently of the applied load. As in the same lapse the sample density does not stop increasing with time, it is reasonable to assume that the examined creep is hindered by stable grain-boundary formation. If so, the dominant creep mechanism should be attributed to instability of particle-to-particle contacts. Actually, as shown by scanning electron micrography (Fig. 4a), our highly porous MgO samples, during the early stage of sintering ($\sim$ 45 min), seem to undergo grain-boundary disconnections (circled in Fig. 4a). This process is probably due to the inherent instability of the solid/pores system [11, 12], which is certainly enhanced when the porosity is very high.

The dependence of creep strain rate on the applied stress is derived from the data of Fig. 3, by plotting logarithmically $\dot{\varepsilon}_c$ against σ_0 at fixed sintering times. The results are shown in Fig. 5 and yield, to within the experimental error, a family of nearly parallel straight lines. The average slope, n, of such lines is 0.44 ± 0.03. Deviation from these values ($n = 0.64$ at 20 min) is observed only for shorter sintering times, probably in the transition to the isothermal regime.

The evidence that the logarithm of $\dot{\varepsilon}_c$ plots linearly against the logarithm of the applied stress proves that Equation 1 correctly applies to the present data. Furthermore, the fact that the angular coefficient n is less than 1 and practically time-independent is a quite new and unexpected result. First of all the investigated phenomenon is neither amenable to a Nabarro–Herring creep, for which $n = 1$ should be expected [17], nor to a superplastic or plastic-type creep for

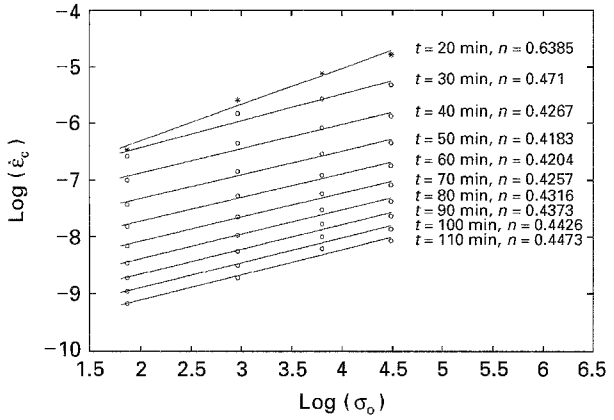

Figure 5 Creep strain rate versus applied stress plotted logarithmically at different firing times. Slopes represent creep exponent n.

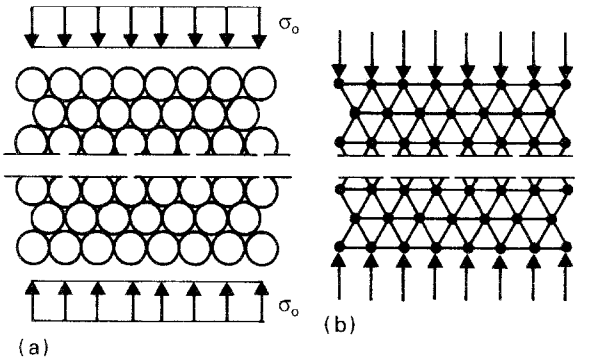

Figure 6 (a) Two-dimensional close-packed sphere aggregate, and (b) its network representation.

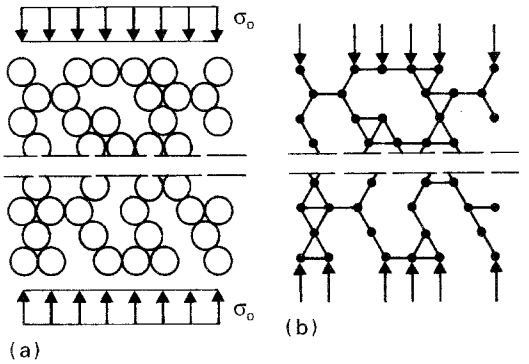

Figure 7 (a) Two-dimensional model of high-porosity sphere aggregate, and (b) its network representation.

which n is equal to or greater than 2 [18]. Secondly, the substantial constancy of the creep exponent with time suggests its weak dependence on the actual density in the explored range (0.28–0.37). Considering that both the mean grain size and the average pore size are uniquely determined by the sample density [9], it should be inferred that the creep exponent is also independent of such variables. Nevertheless a dependence of n on microstructural shape parameters, weakly related to actual density, average pore and grain size, cannot be excluded. If so, the nature of $n < 1$ creep should be due to mechanisms of particle rearrangement and packing changes. Such effects are little related to bulk properties and should be particularly active during the early stage of sintering of highly porous compacts.

4. Physico-mathematical model

A porous compact formed by non-porous particles develops complex states of internal stresses with the progress of a sintering process. This effect is due, partly to the so-called sintering stress which acts locally at the joints between individual particles, as discussed elsewhere [19], and partly to the external load. These stresses tend to concentrate on the neck cross-sections and can be evaluated, at a given instant of the process, by a simplified model, reducing the compact to a topological network where the knots represent the particle centres and each bar is the bond between a couple of considered particles. The network can be studied as an elastic lattice, where the bars are assigned elastic rigidities in connection with the size of the particles and the joints. The effect of internal loads (i.e. the sintering stress) can be studied by imposing appropriate thermal constraints to the system. For example, a uniform sintering stress, Σ, is equivalent to a uniform negative change of temperature. If the porous compact is under the action of an external load, the situation is simulated by application of point forces to the boundary knots. It is quite evident that, in general, both the internal and the external loads can give rise to normal and shear forces, bending moments and torques in the bars. The amount of such actions, exerted on a given joint interface, i.e. a given bar of the lattice, depends in a complicated way on the geometry of the system and could be evaluated by the aid of numerical analysis. For the present purpose a few general remarks will be sufficient.

If the particles are uniform in size and closely packed (Fig. 6a and b) the dominant action is normal force, while bending moments are negligible [20]. Such a situation is typical of high-density porous systems. In the case we are dealing with, i.e. that of a high-porosity system, the network is largely defective (Fig. 7a and b). In this network the effect of bending moments becomes important. We shall see how these bending moments can be responsible for particle rearrangement, and how this mechanism explains a creep exponent less than unity.

Experimental evidence proves that densification and creep start simultaneously. This means that the green compact is a system of mechanically interlocked particles where no rearrangement of the grains is possible under the action of weak applied forces. The contacts between particles will be assumed to be elastic with stresses of the Hertzian-type applied to finite contact regions. At the sintering temperature, neck formation starts from these regions which grow into grain-boundary interfaces. The state of stress also includes in such case the sintering stress, Σ, which was shown elsewhere to be a true stress [19]. Now the lattice model holds. In the absence of bending moment, the true compressive stress acting on a joint interface is substantially uniform and equal to

$$\sigma = N/A + \Sigma \qquad (4)$$

where A is the joint cross-sectional area. The effect of a bending moment M acting on the joint is to generate a stress gradient. A linear Navier–Bernoulli stress distribution [21]

$$\sigma(x) = \frac{N}{A} + \Sigma + \frac{M}{J}x \tag{5}$$

can be assumed, where x is the distance from the centroid of the joint in the direction of the gradient, A is the cross-sectional area and J the second moment of area of the joint.

Both N and M are proportional to the nominal applied stress, σ_0; in particular, we can write

$$N = \psi(G)\phi^2\sigma_0\pi r_0^2 \tag{6}$$

where r_0 is the mean particle radius, $\psi(G)$ is a factor related to the system geometry, and $\phi^2(\rho)$ is a stress concentration factor accounting for the presence of voids [5], a function of the actual relative density. The bending moment can be related to the normal force by

$$M = \chi(G)Nr_0 = \chi(G)\psi(G)\phi^2\sigma_0\pi r_0^3 \tag{7}$$

where, besides the known symbols, $\chi(G)$ is another geometrical factor related to the shape and the degree of connection of the elastic network, equal to zero in the case corresponding to a closed-packed particle arrangement, and of the order of unity for a highly defective bar network (corresponding to a high-porosity compact). As an example, for the simple two-dimensional, one-degree-of-freedom network of Fig. 8, one would easily calculate

$$\psi(G) = \frac{1}{2\cos\alpha} \tag{8a}$$

$$\chi(G) = \frac{3}{8}\operatorname{tg}\alpha \tag{8b}$$

where α is the angle describing the shape of the system.

The ratio between the maximum bending stress and the compressive stress produced by the normal force, N, alone in Equation 5 turns out to be $\chi(G)ar_0/r_i^2$ where a is the mean cross-sectional neck radius and r_i the gyratory radius being a fraction of a. The ratio can be considerably larger than unity in the early stage of sintering, when $r_0 \gg a$: this means that a region of the neck can be submitted to a tensile stress or, at least, to a compressive stress which is far lower than Σ.

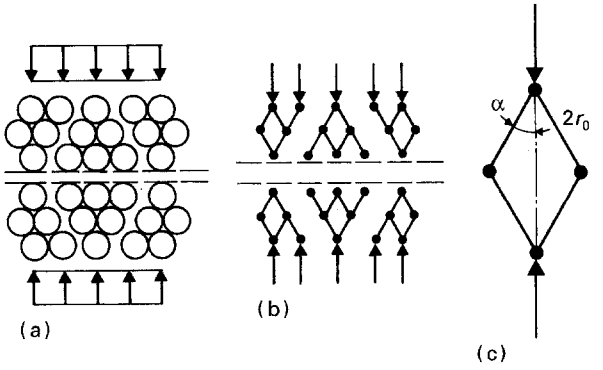

Figure 8 (a) Two-dimensional model of one-degree-of-freedom high-porosity aggregate, (b) its network representation, and (c) unit element of (b).

The stress gradient associated with the distribution of Equation 5 will engender a gradient of chemical potential at the joint interface, given by [19]

$$\frac{\partial\mu}{\partial x} \approx \frac{\partial\sigma}{\partial x}\Omega_0 \approx \frac{M\Omega_0}{J} = \frac{\xi(G)\phi^2\sigma_0\pi r_0^3\Omega_0}{J} \tag{9}$$

where Ω_0 is the atomic volume and $\xi(G) = \psi(G)\chi(G)$ and the free-stress chemical potential has been assumed to be constant on the neck cross-section.

This gradient will produce a diffusional net matter flow in the stressed domain of the joint from the more compressed toward the less compressed region. Thus the two particles undergo a deformation concentrated in the region of the neck which, if allowed by the system geometry, results in a reciprocal tilt or sliding, depending on the dominant diffusion mechanism (Fig. 9). If the shape of the particle is at least approximately conserved, as it is the case during an early stage of sintering, the kinematics of the two-particle system can be described just in terms of an angle α, formed by the lines joining the two centres before and after the movement (Fig. 9a). The local movements in a system containing large voids will give rise to a global rearrangement of the particle network. In this global movement the total volume should remain substantially unchanged, while large shape changes can take place. Following this picture of the creep phenomenon in a highly porous material, it will be possible to establish a relation between the global creep strain and the local kinematic parameter, α, namely

$$\varepsilon_c = f(\alpha, G) \tag{10}$$

where G recalls a general geometry dependence. In the particular case of the four-particle model illustrated in Fig. 8c, this function becomes

$$\varepsilon_c = \frac{4}{3}\frac{\sin(\alpha_0 - \alpha)}{\sin 2\alpha_0} \tag{11}$$

where α_0 is the initial (green) value of α, which expresses the geometry dependence in this special instance.

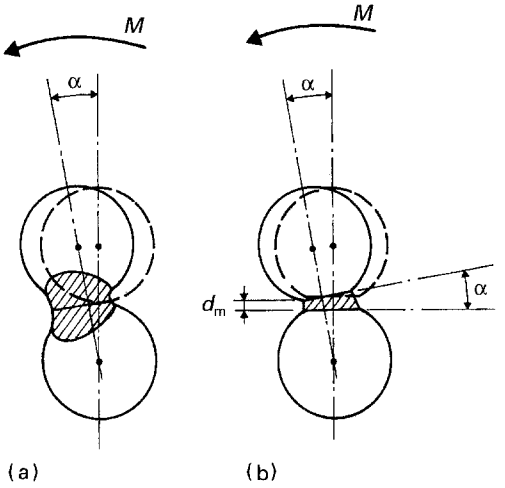

Figure 9 (a) Mechanism of grain-boundary disconnection and two-particle tilting; (b) geometrical model.

The model dependence of the creep strain is certainly a weak point of any analytical model trying to describe the kinetic part of the process. An understanding of the physics of the creep phenomenon, in particular the meaning of the creep exponent, is possible, as we shall prove below, by treating only local variables which are independent of the global geometrical model.

If the diffusion mechanism is such to produce a local axial strain rate, $\dot{\varepsilon}$, proportional to the corresponding local effective stress , $\sigma(x)$, as suggested elsewhere [5, 19] for bulk diffusion, we shall have, for the points of the joint interface

$$\frac{\dot{\varepsilon}(x)}{\sigma(x)} = \frac{\dot{\varepsilon}_d}{\Sigma} \tag{12}$$

where $\dot{\varepsilon}_d$ and Σ are respectively the densification strain rate and the sintering stress at the centroid of the interface ($x = 0$), where the effect of the bending moment, M, is not felt. As the densification rate appeared from experiment to be load independent, the local $\dot{\varepsilon}_d$ can be assumed to coincide with the macroscopic densification strain rate. Furthermore, the gradient of $\dot{\varepsilon}$ represents the rate of bending curvature of the neck cross-section and must be compatible with the rate of tilt, $\dot{\alpha}$, through a simple relation of the type

$$\frac{2\dot{\alpha}}{d_n} = \frac{\partial \dot{\varepsilon}}{\partial x} \tag{13}$$

where d_n is an average depth of the neck region where the bulk diffusion phenomena take place.

From Equations 12 and 13, taking into account Equation 9, one obtains

$$\frac{2\dot{\alpha}}{d_n} = \frac{\partial \sigma}{\partial x}\frac{\dot{\varepsilon}_d}{\Sigma}$$

$$= \frac{\xi(G)\,\phi^2\,\sigma_0 \pi r_0^3}{J}\frac{\dot{\varepsilon}_d}{\Sigma} \tag{14}$$

Eliminating $\dot{\alpha}$ through Equation 10, the ratio of the creep rate to the densification rate can be calculated as

$$\frac{\dot{\varepsilon}_c}{\dot{\varepsilon}_d} = \frac{\phi^2 \sigma_0 \pi r_0^3 d_n}{2\Sigma J} f_\alpha(\alpha, G)\xi(G) \tag{15}$$

where $f_\alpha(\alpha, G)$ is the partial derivative of f with respect to α.

Among the variables on the right-hand side of Equation 15, only the moment of area of the neck cross-section is dependent on the applied stress, σ_0. Because we are dealing only with the relationship between $\dot{\varepsilon}_c$ and σ_0, this relationship must be expressed.

As illustrated in Fig. 10 the effect of the stress distribution on the growth of the neck cross-section is such that the initial contact circle of radius a_0 can expand freely in three directions, but remains practically the same in the region where the applied stress is considerably lower than Σ. Accordingly, a reasonable figure for J is

$$J = \pi a_0^p a^{4-p}/4 \tag{16}$$

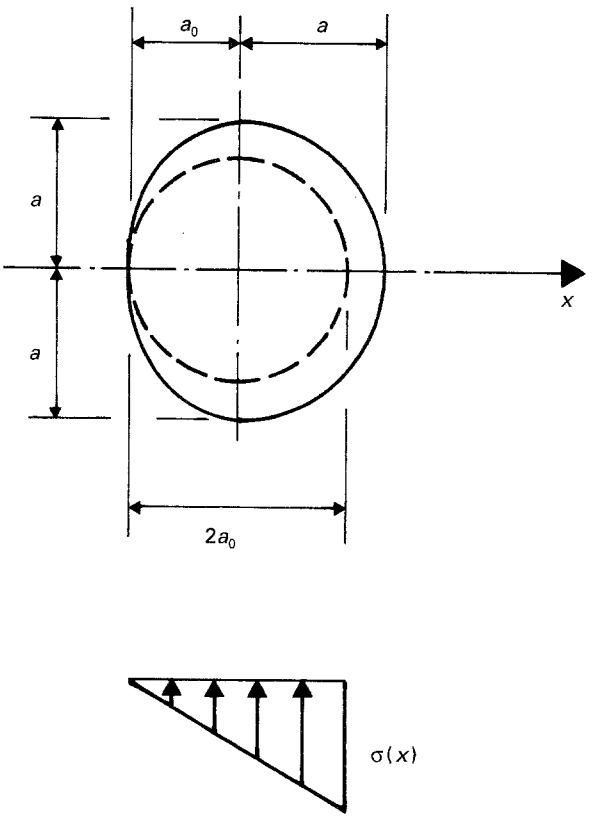

Figure 10 Model of neck growth under non-uniform stress.

where p is an exponent equal to zero in the case of isotropic growth, i.e. in the absence of bending moment, and ranging between 1 and 2 in the other cases. The value of p is expected to be the higher, the larger is the stress gradient on the neck cross-section, i.e. the larger is the effect of bending.

The value of a_0 can be calculated from the Hertzian elastic theory [22] which, for a pair of equal spheres of radius r_0, gives

$$a_0 = \left(\frac{3}{4}\frac{N r_0}{E'}\right)^{1/3} \tag{17}$$

where $E' = E/(1 - \nu^2)$, E being the elastic modulus of the material and ν the Poisson's ratio. The radius a, which results from free sintering, is independent of the applied stress, being a function of the actual density, ρ.

After eliminating N via Equation 6, Equations 17 and 16 can be substituted in Equation 15, which takes the final form

$$\dot{\varepsilon}_c = \dot{\varepsilon}_d \frac{d_n}{r_0}\left(\frac{\sigma_0}{E'}\right)^{1-p/3}\frac{E'}{\Sigma} F(\rho, \varepsilon_c, G) \tag{18}$$

where F is a function now including the kinetic part of the process and the geometry dependence.

5. Discussion

The model described in the foregoing section provides a relation (Equation 18) between the creep strain rate and the densification rate, which depends on a function, F, of the actual microstructure and geometry. Unfortunately, a knowledge of such a function is difficult to obtain either from theory or from experiment.

Therefore, the physico-mathematical model allows, for the present, no prediction of the kinetic law of creep.

Nevertheless, Equation 18 can be used to explore the effect of the applied stress on the creep rate. Generally speaking this dependence, expressed by the value of exponent n in Equation 1, could be regarded as a function of microstructure as well as green density. For the samples we are dealing with, the microstructure appears to be determined only by the actual density [9]. In this framework, the physico-mathematical model allows us to estabish whether in the early stage of sintering the green density or the actual density is the more relevant parameter to the value of n. In fact, from Equation 18 the creep exponent is

$$n = 1 - p/3 \tag{19}$$

where p is a parameter accounting for the anisotropic neck growth due to the action of load-induced bending moments.

When the model is applied to low-porosity compacts, the effect of bending in the bars of the elastic lattice is negligible (Fig. 6). Under such conditions the model predicts $p = 0$ and $n = 1$. The prediction is consistent with experiments of Rahaman *et al.* [3, 6] on high-density compacts of ceramic oxides.

In high-porosity compacts, the effect of bending causes p to assume a value between 1 and 2, with an average of 1.5, corresponding to $n \approx 0.5$. This conclusion compares with the experimental results reported in the present paper, which give $n = 0.44 \pm 0.03$.

In the early stage of sintering, the compact porosity is determined essentially by the green porosity: high-(low-)porosity green samples give high-(low-)porosity sintered compacts. Thus as far as the above model is applied to an early stage of sintering, it will be sufficient to study the meaning of p in connection with its green-density dependence.

Samples with higher green density (about 0.44), treated for the same degree of densification as before, exhibit (Fig. 11) values of n in the range 0.7–1.0, corresponding to p in the range 1.0–0. This means that mechanisms of particle disconnection and rearrangement are the less important, the higher is the green density. This conclusion, which is quite sound, is also supported by SEM observations. In Fig. 4b, the microstructure of MgO after firing exhibits a lower number of particle disconnections than visible in Fig. 4a, which illustrates a more porous compact.

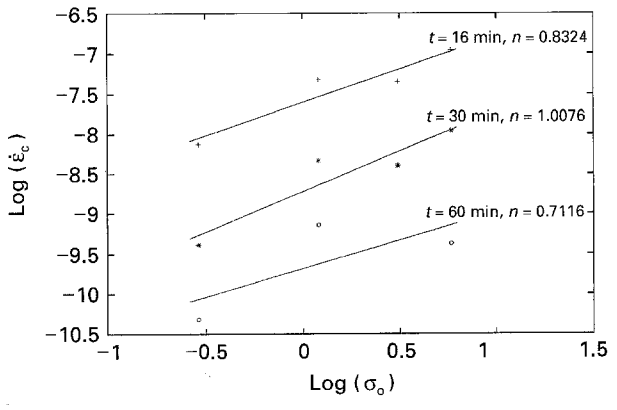

Figure 11 Creep exponents from creep strain rate versus stress for high-density compacts.

Another point, not yet investigated experimentally but clearly implied by Equation 18, is the dependence of the creep rate on the elastic modulus of the material when the creep exponent is less than unity. This dependence totally disappears if $n = 1$.

As a concluding remark on the local nature of the creep phenomena under inquiry, one should recall some conclusions from previous work [5,9]. As far as the temperature dependence is concerned, densification and creep exhibit an equal total apparent activation enthalpy, which suggests a common mechanism of matter transport. For the microstructural dependence, the ratio of densification and creep rate is independent of actual density for high-density compacts, but is an increasing function of ρ in the case of high-porosity compacts. Following Equation 18, the kinetic function, F, should then be different in the two cases and, in particular, it should become insensitive to microstructure in the case of high-density samples.

Acknowledgements

The authors thank Professor A. W. Searcy for his valuable contribution in discussing and improving the manuscript. This work has been supported by the National Council of Researches under the Progetto Finalizzato Materiali Speciali per Tecnologie Avanzate and, partially, by the Ministry of University and Scientific Research (MURST) under the 40% Grant Donation.

References

1. M. N. RAHAMAN and L. C. DE JONGHE, *J. Am. Ceram. Soc.* **67** (1984) C-205.
2. M. N. RAHAMAN, L. C. DE JONGHE and R. J. BROOK, *ibid.* **69** (1986) 53.
3. M. N. RAHAMAN and L. C. DE JONGHE, *ibid.* **70** (1987) 360.
4. *Idem, J. Mater. Sci.* **22** (1987) 4326.
5. L. C. DE JONGHE and M. N. RAHAMAN, *Acta Metall.* **36** (1988) 223.
6. M. N. RAHAMAN, L. C. DE JONGHE and M. Y. CHU, *J. Am. Ceram. Soc.* **74** (1991) 514.
7. M. Y. CHU, M. N. RAHAMAN, L. C. DE JONGHE and R. J. BROOK, *ibid.* **74** (1991) 1217.
8. R. RAJ, *ibid.* **69** (1986) 58.
9. D. BERUTO, A. W. SEARCY, R. BOTTER and M. GIORDANI, to be published.
10. J. E. BIRD, A. K. MUKHERJEE and J. F. DORN, in "Quantitative Relation Between Properties and Microstructure", Haifa, Israel, 4 July–4 August, 1969 (Israel University Press, 1969) pp. 225–342.
11. S. L. DOLE, S. PROCHAZKA and H. DOREMUS, *J. Am. Ceram. Soc.* **72** (1989) 958.
12. B. WONG and J. A. PASK, *J. Am. Ceram. Soc.* **62** (1979) 141.
13. D. BERUTO, R. BOTTER and A. W. SEARCY, *J. Am. Ceram. Soc.* **72** (1989) 232.
14. *Idem*, "The Influence of Thermal Cycling on Densification: Further Test of a Theory", in "Ceramic Transactions", Vol. **1B,** edited by G. L. Messing, E. R. Fuller and H. Hausner (American Ceramic Society, Columbus, OH, 1988).

15. *Idem, J. Am. Ceram. Soc.* **70** (1987) 155.
16. M. Y. CHU, L. C. DE JONGHE and M. N. RAHAMAN, *Acta Metall.* **37** (1989) 1415.
17. R. L. COBLE, *J. Appl. Phys.* **34** (1963) 1679.
18. J. WEERTMAN, *ibid.* **26** (1955) 1213.
19. D. BERUTO and M. CAPURRO, *J. Mater. Sci.* **28** (1993) 4693.
20. S. P. TIMOSHENKO and D. H. YOUNG, "Theory of structures" (McGraw-Hill, New York, London, 1965).
21. R. BALDACCI, "Scienza delle Costruzioni I" (UTET, Torino, 1970).
22. L. LANDAU and E. LIFCHITZ, "Théorie de l'élasticité", (Mir, Moscow, 1967).

Received 11 April 1994
and accepted 17 March 1995